CHANNEL-AWARE ORTHOGONAL PRECODER FOR SIDELOBE SUPPRESSION IN OFDM

Vahid Vahidpour[*], *Roberto López-Valcarce*[*]

atlanTTic, Universidade de Vigo, Spain
{vahidpour,valcarce}@gts.uvigo.es

Josep Sala-Álvarez[†]

Universitat Politècnica de Catalunya, Spain
josep.sala@upc.edu

ABSTRACT

We present a channel-aware spectral precoding framework for multicarrier modulation minimizing weighted leakage in prescribed frequency bands via a semi-unitary precoder. Its right-unitary invariance is exploited to embed channel state information at the transmitter without altering the power spectral density (PSD). By right-unitary rotations through singular value and geometric mean decompositions, we respectively derive low-complexity zero-forcing and successive-interference cancellation based decoders. A closed-form PSD characterization enables rigorous out-of-band radiation analysis and comparison with former pre-equalized and spectrally precoded OFDM (PSP-OFDM) and null-subcarrier schemes. Simulations over block-fading multipath channels demonstrate substantially stronger sidelobe suppression and improved error rates at medium/high SNR. The results establish channel-aware spectral precoding as a principled, efficient solution to joint spectrum and reliability control.

***Index Terms*—** OFDM, spectral precoding, sidelobe suppression, channel state information at transmitter

1. INTRODUCTION

Orthogonal frequency-division multiplexing (OFDM) is widely adopted thanks to its robustness to multipath, flexible spectrum aggregation, and seamless MIMO integration. A well-known drawback is the slow f^{-2} sidelobe decay of rectangularly pulsed OFDM, which produces significant out-of-band radiation (OBR) and adjacent-channel interference [1]. Naively deactivating edge subcarriers is inefficient because sidelobes decay slowly and throughput is sacrificed.

OBR mitigation has been pursued via time-domain and frequency-domain processing. Time-domain shaping, filtering, windowing, and related variants [2–5] can reduce OBR but often require longer guard intervals for a given channel delay spread (thus hurting rate), or expend extra power not useful for data detection. Frequency-domain approaches manipulate symbols before the inverse fast Fourier transform (IFFT), and include nonlinear mapping [6], cancellation carriers [7, 8], and linear precoding [9–15], which provides better OBR reduction levels. Three families dominate: (i) *spectral nulling* (SN), which places notches at specific frequencies outside the passband; (ii) N*-continuous precoding*, enforcing signal smoothness at the symbol boundaries of the time-domain signal; and (iii) *band-specific power minimization* (BSPM), which explicitly minimizes leakage in protected bands. Because precoding spreads symbols across subcarriers, all three can exploit frequency diversity and improve error rates on selective channels [12, 16, 17], albeit with higher receiver complexity than one-tap equalization. Recent structured designs further integrate pilot protection and low-complexity cancellation [15].

Channel-state information at the transmitter (CSIT) has also been fused with spectral precoding in [18] to improve the error rate at the receiver. The pre-equalized and spectrally precoded (PSP)-OFDM design from [18] cascades a spectral kernel of the N-continuous family, a CSIT-driven water-filling stage, and a unitary stage for PAPR reduction, and applies linear minimum mean squared error (LMMSE) decoding at the receiver.

Given the good performance in terms of OBR reduction demonstrated by linear precoding, we propose a novel BSPM-based, CSIT-aware design for linear spectral precoding with an orthogonal precoding matrix. This design exploits right-unitary precoder invariance to embed CSIT without changing the power spectral density (PSD), and obtains low-complexity zero-Forcing (ZF) or Successive Interference Cancellation (SIC) receivers, respectively via a singular value (SVD) or geometric mean decomposition (GMD) of the effective channel. We provide rigorous OBR comparisons against PSP-OFDM and null-subcarrier baselines. Simulations over block-fading multipath channels show markedly stronger edge-band suppression and improved mid/high-SNR error rate, while avoiding PSP-OFDM's water-filling stage.

Notation: a, $\mathbf{a}$, and $\mathbf{A}$ represent scalar, vector and matrix, resp.; $\mathbf{A}^{\mathsf{T}}$, and $\mathbf{A}^{\mathsf{H}}$ resp. denote transpose and conjugate transpose. $\mathbb{A} \subset \mathbb{C}$ denotes the signal constellation. The trace of a square matrix $\mathbf{A}$ is $\mathsf{Tr}(\mathbf{A})$. $\mathsf{E}[\cdot]$ denotes statistical expectation. The hard-decision operator $\mathsf{DEC}_{\mathbb{A}}\{\cdot\}$ maps a vector to $\mathbb{A}$ componentwise.

[*]Supported by MICIU/AEI/10.13039/501100011033 and by ERDF/EU under grant PID2022-136512OB-C22.

[†]Supported by MICIU/AEI/10.13039/501100011033 and by ERDF/EU under grant PID2022-136512OB-C21.

2. SIGNAL MODEL

Consider a multicarrier communication system with an IFFT of size N and a guard interval of l_g samples. Let the set of active subcarriers be $\mathcal{K} = \{k_1, \ldots, k_K\}$ with $|\mathcal{K}| = K \leq N$, and define the block length $L \triangleq N + l_g$. At OFDM block time m, collect $D \leq K$ information symbols into $\mathbf{d}_m \triangleq \left[d_1^{(m)}, \ldots, d_D^{(m)}\right]^{\mathsf{T}} \in \mathbb{A}^D$. A (memoryless) linear spectral precoder $\mathbf{G} \in \mathbb{C}^{K\times D}$ maps $\mathbf{d}_m$ to the K active subcarriers:

$$\mathbf{x}_m = \mathbf{G}\mathbf{d}_m \in \mathbb{C}^K. \tag{1}$$

We denote the coding rate and redundancy by $\lambda = D/K \leq 1$ and $R \triangleq K - D \geq 0$, respectively. Let $x_k^{(m)}$ be the entry of $\mathbf{x}_m$ associated with subcarrier $k \in \mathcal{K}$. The discrete-time baseband signal is

$$s[n] = \sum_{m=-\infty}^{\infty} \sum_{k\in\mathcal{K}} x_k^{(m)} h_{\mathrm{P}}[n - mL] \mathrm{e}^{\jmath \frac{2\pi}{N} k(n-mL)}, \tag{2}$$

where $h_{\mathrm{P}}[n]$ is the shaping pulse, with discrete-time Fourier transform (DTFT) $H_{\mathrm{P}}(\mathrm{e}^{\jmath\omega}) = \sum_{n=-\infty}^{\infty} h_{\mathrm{P}}[n]\mathrm{e}^{-\jmath\omega n}$. For instance, for cyclic prefix (CP) based OFDM with a length-L rectangular pulse, $h_{\mathrm{P}}[n] = 1$ for $0 \leq n < L$ and 0 otherwise; the model captures other variants such as zero-padded (ZP) OFDM, etc. [19]. After parallel-to-serial and digital-to-analog conversion at $f_s = 1/T_s$ samples/s using an interpolation filter $h_{\mathrm{I}}(t)$ with frequency response $H_{\mathrm{I}}(f) \triangleq \int_{-\infty}^{\infty} h_{\mathrm{I}}(t)\, \mathrm{e}^{-\jmath 2\pi f t}\, \mathrm{d}t$, the subcarrier spacing is $\Delta_f \triangleq 1/(NT_s)$ (Hz), and the continuous-time waveform is

$$s(t) = \sum_{n=-\infty}^{\infty} s[n] h_{\mathrm{I}}(t - nT_s). \tag{3}$$

Assume that the data vector $\mathbf{d}_m$ is zero-mean and temporally white/uncorrelated with covariance $\mathsf{E}\big[\mathbf{d}_m\mathbf{d}_{m-\ell}^{\mathsf{H}}\big] = \delta[\ell]\mathbf{I}_D$. Define spectral shape at the k-th subcarrier as $\phi_k(f) \triangleq H_{\mathrm{P}}^*(\mathrm{e}^{\jmath 2\pi(f-k\Delta_f)T_s})$ and stack them as $\boldsymbol{\phi}(f) \triangleq [\phi_{k_1}(f), \ldots, \phi_{k_K}(f)]^{\mathsf{T}} \in \mathbb{C}^K$. Invoking [19, Th. 1], the continuous-time process $s(t)$ in (3) is wide-sense cyclostationary with period LT_s, and has PSD given by

$$P_s(f) = \frac{|H_{\mathrm{I}}(f)|^2}{LT_s} \boldsymbol{\phi}^{\mathsf{H}}(f)\mathbf{G}\mathbf{G}^{\mathsf{H}}\boldsymbol{\phi}(f). \tag{4}$$

3. PROBLEM STATEMENT

For a nonnegative weighting function $W(f) \geq 0$, define the weighted transmit power

$$P_W \triangleq \int_{-\infty}^{\infty} W(f) P_s(f) \mathrm{d}f = \mathsf{Tr}\Big(\mathbf{G}^{\mathsf{H}}\boldsymbol{\Phi}\mathbf{G}\Big), \tag{5}$$

where the positive semidefinite matrix $\boldsymbol{\Phi} \in \mathbb{C}^{K\times K}$ is

$$\boldsymbol{\Phi} \triangleq \frac{1}{LT_s} \int_{-\infty}^{\infty} W(f)|H_{\mathrm{I}}(f)|^2 \boldsymbol{\phi}(f)\boldsymbol{\phi}^{\mathsf{H}}(f)\mathrm{d}f. \tag{6}$$

Our goal is to minimize OBR over a prescribed frequency region $\mathcal{B}$. This is achieved by selecting $W(f)$ supported on $\mathcal{B}$; for uniform emphasis within $\mathcal{B}$ one may set $W(f) = 1$ for $f \in \mathcal{B}$ and zero elsewhere, whereas nonuniform choices $W(f) \geq 0$ can prioritize specific subbands within $\mathcal{B}$. Notice that some constraint has to be placed on the precoding matrix $\mathbf{G}$ to avoid the trivial solution $\mathbf{G} = \mathbf{0}$; a sensible approach is to constrain $\mathbf{G}$ to be semi-unitary, *i.e.,* to have orthonormal columns [9, 17, 20]. Then the optimization problem reads as

$$\min_{\mathbf{G}} P_W = \mathsf{Tr}\Big(\mathbf{G}^{\mathsf{H}}\boldsymbol{\Phi}\mathbf{G}\Big) \quad \text{s. to } \ \mathbf{G}^{\mathsf{H}}\mathbf{G} = \mathbf{I}_D. \tag{7}$$

The optimal precoder $\mathbf{G}_\star$ has columns spanning the eigenspace associated with the D smallest eigenvalues of $\boldsymbol{\Phi}$ [17], and it is unique up to a right unitary rotation within any eigenspace of repeated eigenvalues.

We now consider the case with CSIT and leverage it to improve receiver error-rate performance. For brevity, we drop the symbol index m and write $\mathbf{d}$ and $\mathbf{x}$ in lieu of $\mathbf{d}_m$ and $\mathbf{x}_m$. Assuming that the channel impulse response is no longer than the guard interval and that it does not change substantially over the duration of the OFDM symbol, the per-subcarrier channel after CP removal and N-point FFT is diagonal:

$$\mathbf{H} \triangleq \mathsf{diag}\left\{H_c[k_1], \ldots, H_c[k_K]\right\} \in \mathbb{C}^{K\times K}, \tag{8}$$

where $H_c[k]$ denotes the N-point DFT sample of the channel impulse response at bin k. Under ideal timing and carrier synchronization, and with no equalization applied yet, the received vector for a precoding matrix $\mathbf{G}$ (optimal or not) is

$$\mathbf{r} = \mathbf{H}\mathbf{x} + \mathbf{n} = \mathbf{H}\mathbf{G}\mathbf{d} + \mathbf{n}, \tag{9}$$

where the circularly-symmetric, zero-mean Gaussian noise vector $\mathbf{n} \in \mathbb{C}^K$ has covariance $\mathsf{E}\big[\mathbf{n}\mathbf{n}^{\mathsf{H}}\big] = \sigma^2\mathbf{I}_K$. Note that, for any unitary $\mathbf{V} \in \mathbb{C}^{D\times D}$, replacing $\mathbf{G}$ by $\mathbf{G}\mathbf{V}^{\mathsf{H}}$ does not alter the transmit signal PSD in (4) and thus the OBR (5). This *right-unitary invariance* exposes a family of equivalent precoders, among which one can choose to improve some system feature while preserving the PSD achieved by $\mathbf{G}_\star$, *e.g.,* on-line complexity [21] or PAPR [18]. Differently, we shall exploit this fact and the availability of CSIT, *i.e.,* knowledge of $\mathbf{H}$ at the transmitter, to design adequate matrices $\mathbf{V}$ depending on the decoding strategy adopted at the receiver.

4. PROPOSED PRECODER DESIGNS

We now detail precoder/receiver designs compatible with the spectrally optimal, semi-unitary precoder $\mathbf{G}_\star$ from Sec. 3. All schemes operate on the input-output relation in (9) and differ only in how they exploit (or ignore) CSIT through a right-unitary rotation of $\mathbf{G}_\star$.

4.1. Zero-Forcing decoder without CSIT

This baseline employs the OBR-optimal semi-unitary precoder from (7) at the transmitter, *i.e.,* $\mathbf{G} = \mathbf{G}_\star$, without exploiting CSIT. The received vector under the per-subcarrier diagonal channel $\mathbf{H}$ is (9). Assuming $\mathbf{H}^{-1}$ exists, the ZF equalizer applies per-subcarrier inversion followed by projection onto the precoder subspace:

$$\mathbf{G}_\star^{\mathsf{H}}\mathbf{H}^{-1}\mathbf{r} = \mathbf{d} + \mathbf{w}, \tag{10}$$

where $\mathbf{w} = \mathbf{G}_\star^{\mathsf{H}}\mathbf{H}^{-1}\mathbf{n} \in \mathbb{C}^D$ is the post-decoding noise. Note that the equalization step (multiplication by $\mathbf{H}^{-1}$) will result in noise enhancement, particularly at subcarriers suffering larger channel attenuation. A component-wise hard decision then yields $\hat{\mathbf{d}} = \mathsf{DEC}_{\mathbb{A}}\{\mathbf{G}_\star^{\mathsf{H}}\mathbf{H}^{-1}\mathbf{r}\}$ to recover each symbol by selecting the nearest constellation point. The post-decoding noise $\mathbf{w}$ remains zero-mean Gaussian, but it is now colored, with covariance $\mathsf{E}[\mathbf{w}\mathbf{w}^{\mathsf{H}}] = \sigma^2\mathbf{G}_\star^{\mathsf{H}}(\mathbf{H}^{\mathsf{H}}\mathbf{H})^{-1}\mathbf{G}_\star$.

4.2. Zero-Forcing decoder with CSIT

With CSIT, we exploit the right-unitary invariance of $\mathbf{G}_\star$ to diagonalize the effective channel. Consider the compact SVD

$$\mathbf{H}\mathbf{G}_\star = \mathbf{U}_c\mathbf{\Gamma}_c\mathbf{V}_c^{\mathsf{H}}, \tag{11}$$

where $\mathbf{U}_c \in \mathbb{C}^{K\times D}$ has orthonormal columns, $\mathbf{\Gamma}_c = \mathsf{diag}\{\gamma_1,\ldots,\gamma_D\} \in \mathbb{R}^{D\times D}$, and $\mathbf{V}_c \in \mathbb{C}^{D\times D}$ is unitary. Then choose the transmit precoder as $\mathbf{G} = \mathbf{G}_\star\mathbf{V}_c$, which yields the received signal

$$\mathbf{r} = \mathbf{H}\mathbf{G}_\star\mathbf{V}_c\mathbf{d} + \mathbf{n} = \mathbf{U}_c\mathbf{\Gamma}_c\mathbf{d} + \mathbf{n}. \tag{12}$$

A ZF decoder removes the semi-unitary mixing and then inverts the diagonal gain:

$$\mathbf{\Gamma}_c^{-1}\mathbf{U}_c^{\mathsf{H}}\mathbf{r} = \mathbf{d} + \mathbf{w}_c, \tag{13}$$

with post-decoding noise $\mathbf{w}_c = \mathbf{\Gamma}_c^{-1}\mathbf{U}_c^{\mathsf{H}}\mathbf{n}$. A hard decision produces the final estimate, $\hat{\mathbf{d}} = \mathsf{DEC}_{\mathbb{A}}\{\mathbf{\Gamma}_c^{-1}\mathbf{U}_c^{\mathsf{H}}\mathbf{r}\}$. Now $\mathbf{w}_c$ is zero-mean Gaussian with covariance $\mathsf{E}[\mathbf{w}_c\mathbf{w}_c^{\mathsf{H}}] = \sigma^2\mathbf{\Gamma}_c^{-2}$. In this case, small singular values γ_i (deep fades within the span of $\mathbf{H}\mathbf{G}_\star$) will cause larger noise enhancement.

4.3. SIC decoder with CSIT

In this case, we leverage the GMD [22] of the effective channel to allow the receiver 'see' a triangular structure that is conducive to SIC decoding. The GMD is given by

$$\mathbf{H}\mathbf{G}_\star = \gamma\mathbf{Q}_c\mathbf{R}_c\mathbf{P}_c^{\mathsf{H}}, \tag{14}$$

where $\mathbf{Q}_c \in \mathbb{C}^{K\times D}$ is semi-unitary, $\mathbf{P}_c \in \mathbb{C}^{D\times D}$ is unitary, $\mathbf{R}_c \in \mathbb{C}^{D\times D}$ is unit upper triangular (*i.e.,* with ones on its diagonal), and γ is the geometric mean of the singular values of $\mathbf{H}\mathbf{G}_\star$: $\gamma = \sqrt[D]{\gamma_1\gamma_2\cdots\gamma_D}$. Then, the spectral precoder is chosen as $\mathbf{G}_\star\mathbf{P}_c$, so that the received signal becomes

$$\mathbf{r} = \mathbf{H}\mathbf{G}_\star\mathbf{P}_c\mathbf{d} + \mathbf{n} = \gamma\mathbf{Q}_c\mathbf{R}_c\mathbf{d} + \mathbf{n}. \tag{15}$$

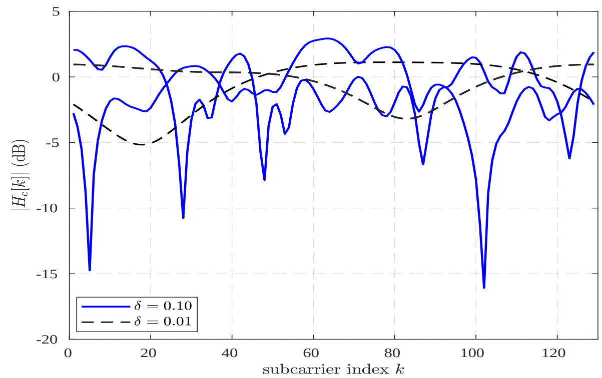

Fig. 1: Channel response $|H_c[k]|$ vs. subcarrier index for four Rayleigh block-fading realizations with $\delta \in \{0.01, 0.10\}$.

Left-multiplying by $\mathbf{Q}_c^{\mathsf{H}}$ and compensating the scaling yields

$$\widetilde{\mathbf{r}} \triangleq \gamma^{-1}\mathbf{Q}_c^{\mathsf{H}}\mathbf{r} = \mathbf{R}_c\mathbf{d} + \widetilde{\mathbf{w}}_c, \tag{16}$$

where $\widetilde{\mathbf{w}}_c = \gamma^{-1}\mathbf{Q}_c^{\mathsf{H}}\mathbf{n}$. Since $\mathbf{Q}_c$ is semi-unitary and $\mathsf{E}[\mathbf{n}\mathbf{n}^{\mathsf{H}}] = \sigma^2\mathbf{I}_K$, the covariance of the post-decoding noise reduces to $\mathsf{E}[\widetilde{\mathbf{w}}_c\widetilde{\mathbf{w}}_c^{\mathsf{H}}] = \frac{\sigma^2}{\gamma^2}\mathbf{I}_D$. Thus, $\widetilde{\mathbf{w}}$ is white with constant per-stream variance σ^2/γ^2. Note that, by virtue of the harmonic mean-geometric mean inequality [23], one has

$$\mathsf{E}\left[\|\widetilde{\mathbf{w}}_c\|^2\right] \le \mathsf{E}\left[\|\mathbf{w}_c\|^2\right]. \tag{17}$$

The triangular structure of $\mathbf{R}_c$ in (16) can now be exploited to obtain the estimate of the data $\mathbf{d}$ based on $\widetilde{\mathbf{r}}$ via SIC. Specifically, let ρ_{pq} denote the (p,q) element of $\mathbf{R}_c$, so that $\rho_{pp} = 1$ and $\rho_{pq} = 0$ for $p > q$. Then, SIC decoding proceeds as:

$$\begin{aligned} \hat{d}_D &= \mathsf{DEC}_{\mathbb{A}}\{\tilde{r}_D\}, \\ \hat{d}_p &= \mathsf{DEC}_{\mathbb{A}}\left\{\tilde{r}_p - \sum_{q=p+1}^{D}\rho_{pq}\hat{d}_q\right\}, \quad p = D-1,\ldots,1. \end{aligned}$$

5. NUMERICAL EXAMPLES

5.1. System configuration

We consider a CP-OFDM setup with rectangular pulses ($h_{\mathrm{P}}[n] = 1$ for $0 \le n < L$, and zero otherwise), IFFT size $N = 256$ and CP length $l_g = N/8 = 32$. The DAC interpolation filter is ideal lowpass, i.e., $|H_{\mathrm{I}}(f)| = 1$ for $|fT_s| \le \frac{1}{2}$ and 0 otherwise. The number of active subcarriers is $K = 129$, arranged symmetrically around the carrier frequency. OBR is penalized over $\mathcal{B} \triangleq \left\{f : \frac{1}{4T_s} + \frac{\Delta_f}{2} \le |f| \le \frac{1}{2T_s}\right\}$, using a flat weight $W(f) = 1$ for $f \in \mathcal{B}$, $W(f) = 0$ for $f \notin \mathcal{B}$.

We adopt a block-fading, finite-length multipath channel model with exponential power-delay profile (PDP) [24]. The discrete-time impulse response is given by

$$h_c[n] = \mathrm{e}^{-\frac{n}{2\delta l_g}}\,\tilde{h}_c[n], \qquad 0 \le n \le l_g - 1 \tag{18}$$

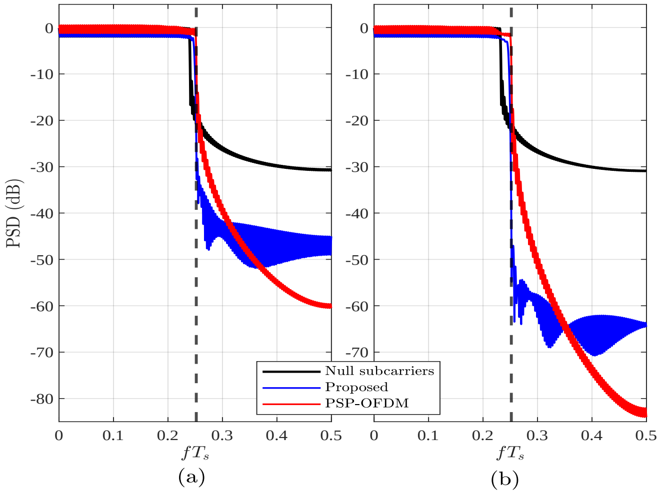

Fig. 2: PSDs of proposed and PSP-OFDM precoders on a multipath block-fading channel with $N = 256$, $l_g = N/8$, $K = 129$ and $\delta = 0.10$; with (a) $R = 6$, and (b) $R = 10$.

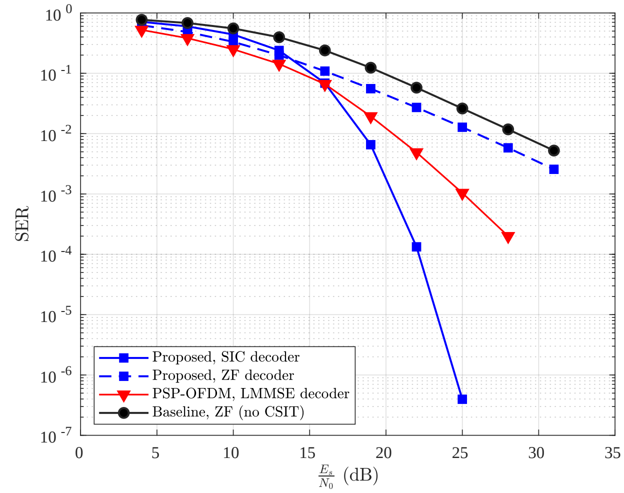

Fig. 3: SER performance of proposed and PSP-OFDM precoders on a multipath block-fading channel for 16-QAM modulation (ZF and SIC), with $\delta = 0.10$ and $R = 6$.

where $\{\tilde{h}_c[n]\}$ are i.i.d. circularly symmetric complex Gaussian variables, and $\delta > 0$ is a dimensionless delay-spread factor. Under (18), δl_g equals both the mean delay and the root-mean-square (RMS) delay spread (in samples) of the exponential PDP. The per-subcarrier channel gains $H_c[k]$ are obtained via the N-point DFT of $\{h_c[n]\}$, and are normalized per realization to enforce a fixed total in-band gain, $\sum_{k\in\mathcal{K}} |H_c[k]|^2 = K$. Fig. 1 shows several channel realizations for two different values $\delta \in \{0.01, 0.1\}$. Clearly, as δ increases the channel becomes more frequency selective.

5.2. Sidelobe suppression performance

Fig. 2 compares the power spectral densities of the proposed BSPM-based precoders, the PSP-OFDM design from [18], and a *null-subcarrier* baseline (obtained by disabling $R/2$ tones at each passband edge) under block-fading multipath channels with significant delay spread ($\delta = 0.10$), for redundancies $R \in \{6, 10\}$. Note that, although the three designs from Sec. 4 use different precoders $\mathbf{G}_\star$, $\mathbf{G}_\star\mathbf{V}_c$, $\mathbf{G}_\star\mathbf{P}_c$, they are all spectrally equivalent in that they provide the same PSD, independently of the channel realization. On the other hand, because PSP-OFDM's precoder depends on the instantaneous channel, we report spectral results as ensemble averages over 1000 independent block-fading realizations. For a fixed R, the proposed designs yield substantially sharper spectra than PSP-OFDM, and sidelobe suppression improves as R increases. Quantitatively, for $R = 6$ PSP-OFDM removes 2.07 dB of out-of-band energy, whereas the proposed schemes achieve 14.95 dB; at $R = 10$ PSP-OFDM attains 4.43 dB vs. 32.19 dB for the proposed designs. Whereas PSP-OFDM benefits from its asymptotic f^{-2R-2} roll-off, the BSPM criterion concentrates suppression where it matters most, right at the passband edges, thereby delivering markedly larger OBR reduction.

5.3. Error rate performance

All symbol error rate (SER) curves are ensemble averaged over 1000 channel realizations. A 16-QAM constellation is assumed without forward-error correction coding. As seen in Fig. 3, all channel-aware schemes outperform the ZF without CSIT baseline, highlighting the benefits of integrating CSIT, if available, in the spectral precoder design.

At low SNR, PSP-OFDM with LMMSE detection (which has knowledge of the noise variance) performs best, while SIC suffers from error propagation. As SNR rises, decisions stabilize and the SER of the proposed SIC-based receiver drops fastest and becomes best from mid SNR upward, leveraging a semi-unitary front-end (no noise gain) and frequency-diversity via the triangular structure. The curve for the ZF with CSIT design sits higher because the ZF decoder amplifies noise on weak subcarriers. Overall, the proposed SIC-based decoder yields the strongest reliability once the SNR is sufficiently high.

6. CONCLUSION

The proposed band-specific spectral precoder designs allow exploiting knowledge of the channel at the transmitter to improve error rate performance at the receiver side, while obtaining very sharp transmit power spectra independent of the channel response. The GMD-based SIC-oriented design exhibits particularly good performance at medium and high SNR, whereas in low SNR it is outperformed by the SVD-based ZF-oriented design due to error propagation.

7. REFERENCES

[1] H. Bogucka, A. M. Wyglinski, S. Pagadarai, and A. Kliks, "Spectrally agile multicarrier waveforms for opportunistic wireless access," *IEEE Commun. Mag.*, vol. 49, no. 6, pp. 108–115, 2011.

[2] J. Park, E. Lee, S.-H. Park, S. Raymond, S. Pyo, and H.-S. Jo, "Modeling and analysis on radio interference of OFDM waveforms for coexistence study," *IEEE Access*, vol. 7, pp. 35132–35147, 2019.

[3] L. Díez, J. A. Cortés, F. J. Cañete, E. Martos-Naya, and S. Iranzo, "A generalized spectral shaping method for OFDM signals," *IEEE Trans. Commun.*, vol. 67, no. 5, pp. 3540–3551, 2019.

[4] M. M. Naghsh, E. Haj Mirza Alian, S. Khobahi, and O. Rezaei, "A majorization–minimization approach for reducing out-of-band radiations in OFDM systems," *IEEE Commun. Lett.*, vol. 21, no. 8, pp. 1739–1742, 2017.

[5] A. Tom, A. Şahin, and H. Arslan, "Suppressing alignment: Joint PAPR and out-of-band power leakage reduction for OFDM-based systems," *IEEE Trans. Commun.*, vol. 64, no. 3, pp. 1100–1109, 2016.

[6] S. Pagadarai, R. Rajbanshi, A. M. Wyglinski, and G. J. Minden, "Sidelobe suppression for OFDM-based cognitive radios using constellation expansion," in *IEEE Wireless Commun. Netw. Conf. (WCNC)*, 2008, pp. 888–893.

[7] S. Brandes, I. Cosovic, and M. Schnell, "Reduction of out-of-band radiation in OFDM systems by insertion of cancellation carriers," *IEEE Commun. Lett.*, vol. 10, no. 6, pp. 420–422, 2006.

[8] J. F. Schmidt, D. Romero, and R. López-Valcarce, "Active interference cancellation for OFDM spectrum sculpting: Linear processing is optimal," *IEEE Commun. Lett.*, vol. 18, no. 9, pp. 1543–1546, 2014.

[9] J. van de Beek, "Orthogonal multiplexing in a subspace of frequency well-localized signals," *IEEE Commun. Lett.*, vol. 14, no. 10, pp. 882–884, 2010.

[10] J. van de Beek and F. Berggren, "N-continuous OFDM," *IEEE Commun. Lett.*, vol. 13, no. 1, pp. 1–3, 2009.

[11] L. Dan, C. Zhang, J. Yuan, P. Wen, and B. Fu, "Improved N-continuous OFDM using adaptive power allocation," in *" in Proc. IEEE 8th Annu. Comput. Commun. Workshop Conf.*, 2018, pp. 937–940.

[12] C.-D. Chung and K.-W. Chen, "Spectrally precoded OFDM without guard insertion," *IEEE Trans. Veh. Technol.*, vol. 66, no. 1, pp. 107–121, 2017.

[13] M. Mohamad, R. Nilsson, and J. Van De Beek, "A novel transmitter architecture for spectrally-precoded OFDM," *IEEE Trans. Circuits Syst. I*, vol. 65, no. 8, pp. 2592–2605, 2018.

[14] R. Kumar, K. Hussain, and R. López-Valcarce, "Mask-compliant orthogonal precoding for spectrally efficient OFDM," *IEEE Trans. Commun.*, vol. 69, no. 3, pp. 1990–2001, 2021.

[15] K. Hussain, R. López-Valcarce, F. Rey, J. Sala-Alvarez, and J. Villares, "Sidelobe suppression for multicarrier signals via structured spectral precoding," *IEEE Trans. Commun.*, vol. 72, no. 6, pp. 3155–3168, 2024.

[16] H.-M. Chen, W.-C. Chen, and C.-D. Chung, "Spectrally precoded OFDM and OFDMA with cyclic prefix and unconstrained guard ratios," *IEEE Trans. Wireless Commun.*, vol. 10, no. 5, pp. 1416–1427, 2011.

[17] M. Ma, X. Huang, B. Jiao, and Y. J. Guo, "Optimal orthogonal precoding for power leakage suppression in DFT-based systems," *IEEE Commun. Lett.*, vol. 59, no. 3, pp. 844–853, 2011.

[18] W.-C. Chen, C.-D. Chung, and P.-H. Wang, "Pre-equalized and spectrally precoded OFDM," *IEEE Trans. Veh. Technol.*, vol. 71, no. 7, pp. 7472–7486, 2022.

[19] R. López-Valcarce, "General form of the power spectral density of multicarrier signals," *IEEE Trans. Commun.*, vol. 26, no. 8, pp. 1755–1759, 2022.

[20] K. Hussain and R. López-Valcarce, "Orthogonal precoding with memory for sidelobe suppression in OFDM," in *Eur. Signal Process. Conf. (EUSIPCO)*, 2022, pp. 1646–1650.

[21] I. V. L. Clarkson, "Orthogonal precoding for sidelobe suppression in DFT-based systems using block reflectors," in *Proc. IEEE Int. Conf. Acoust., Speech, Signal Process.*, 2017, pp. 3709–3713.

[22] J. Yi, W. H. William, and L. Jian, "The geometric mean decomposition," *Linear Algebra Appl.*, vol. 396, pp. 373–384, 2005.

[23] G. H. Hardy, J. E. Littlewood, and G. Pólya, *Inequalities*, Cambridge University Press, Cambridge, UK, 2nd edition, 1952.

[24] H. Arslan and T. Yucek, "Delay spread estimation for wireless communication systems," in *Proc. IEEE 8th Symp. Comput. and Commun.*, 2003, pp. 282–287.